EXPERIMENTAL MODELLING OF BURIED CONTINUOUS PIPELINES CROSSING STRIKE-SLIP FAULTS

H. E. Demirci[(1)], S. Bhattacharya[(2)], M. Karaman[(3)], G. Nikitas[(4)]

[(1)] *PhD Candidate, University of Surrey, hasanemredemirci@gmail.com*
[(2)] *Professor, University of Surrey, s.bhattacharya@surrey.ac.uk*
[(3)] *PhD Candidate, Izmir Institute of Technology, mustafakaraman@iyte.edu.tr*
[(4)] *PhD Candidate, University of Surrey, georgios.nikitas@surrey.ac.uk*

Abstract

A large number of buried pipelines are located in seismically active regions. Earthquake related pipeline damage can severely affect a nation's industries, economy, and services. Thus, earthquake resistant design of buried continuous pipelines is one of the significant aspects of geotechnical and structural engineering. Fault movement is one of the main seismic hazards that causes different types of pipe failure mechanisms. Types of failures include joint failure, tension failure, beam buckling and local (shell) buckling. The repair costs of the pipeline damage are extremely expensive if the damage occurs at a large scale as a result of seismic hazard. In this study, relevant scaling laws and non-dimensional groups governing the pipeline behavior under strike-slip faulting are derived to design an experimental setup to simulate the soil-structure interaction problem. A newly developed test setup of buried continuous pipelines crossing strike-slip faults is also presented. Finally, typical test results in terms of bending and axial pipe strains are presented to assess the performance of the proposed test setup.

Keywords: strike-slip faults, buried continuous pipelines, earthquake, physical modeling

1. Introduction

Pipelines crossing active faults experienced severe damage in past earthquakes. Fault rupture is one of the major seismic hazards that endanger the pipeline integrity. Pipeline failures significantly influence a nation's economy, services, and industries in terms of pollution, fuel loss and flow interruption. The assessment of a pipeline performance under active faults has become the main focus of researchers and a considerable amount of studies including analytical, numerical and experimental have been done to investigate the response of pipelines to active faults in the last five decades. [1], [2], [3], [4], [5], [6] and [7] developed analytical methodologies to predict bending and axial strains within buried continuous pipelines crossing strike-slip and normal faults. Finite Element (FE) method based numerical models were developed by several researchers to simulate pipelines crossing active faults ([8], [9], [10], [11], [12], [13], [14], [15]) and further details can be found in [30]. These numerical models were used for: a) the investigation of the performance of pipelines crossing active faults, b) the investigation of the parameters affecting the behavior of pipelines crossing active faults and c) the evaluation of the performance of seismic mitigation techniques for buried pipelines subjected to fault rupture. Several experimental research including centrifuge, large-scale and small-scale tests were conducted to investigate the effects of faulting on pipelines crossing active faults ([16], [17], [18], [19], [20], [21], [22] and [15]). These experiments were performed to investigate pipeline performance under faulting, explore the parameters influencing the behavior of pipelines crossing active faults, and validate numerical and analytical models.

In this paper, a new experimental setup that is developed to investigate the effects of strike-slip faults on buried continuous High-Density Polyethylene (HDPE) pipelines is described. The relevant non-dimensional groups and scaling laws for buried pipelines crossing active faults are derived. The physical meaning and practical range of governing non-dimensional groups are provided. Typical test results are presented by using non-dimensional groups and results of four model tests in terms of axial and bending strains are presented to

investigate the effects of pipe burial depths and fault crossing angles on pipeline response to strike-slip faulting.

2. Experimental Modelling

Buried pipelines crossing strike-slip faults experience lateral and axial soil reactions due to relative movement between pipelines and soil surrounding them. Buried pipelines bend at either side of faults (as shown in Figure 1a) due to fault movement and curved pipeline section (red line in Figure 1a) is therefore developed. Lateral soil reaction (P_u) occurs at the soil-pipe interface throughout the curved pipeline parts. Axial soil reaction (T_u) occurs along the soil-pipeline interface due to axial relative displacements between the soil and pipeline. At anchor points (shown in Figure 1a-b), axial soil-pipe friction forces become zero. These lateral and axial soil pipe interactions are modeled by using lateral (P-z) and axial (T-x) soil springs as shown in Figure 1b. Anchor points are specified considering unanchored length (L_a) and the anchor points are pinned. The force-displacement relationships for lateral and axial soil springs are shown in Figure 1c.

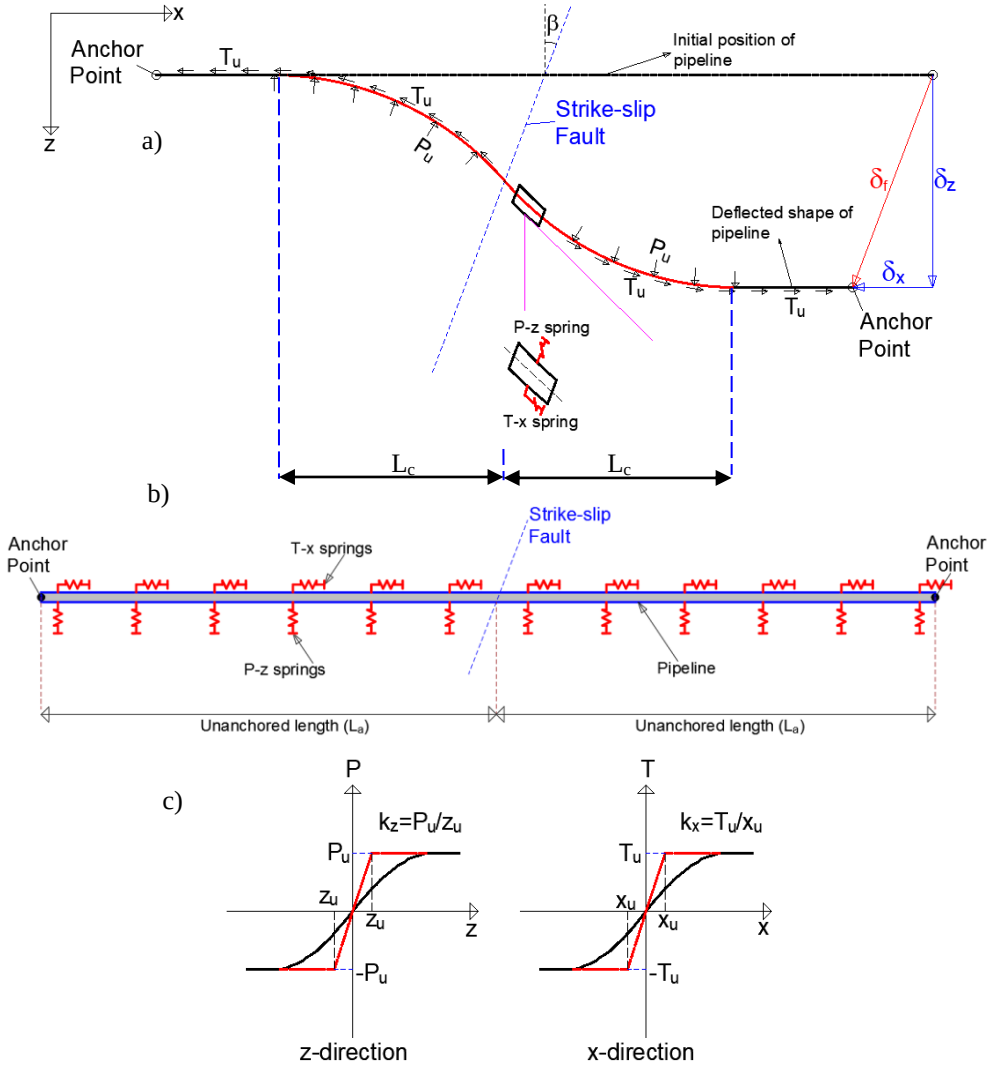

Fig. 1 – a) Forces acting on pipelines crossing strike-slip faults, b) the schematic sketch of a simple numerical model of buried continuous pipelines crossing strike-slip faults, c) force-displacement relationships for lateral (z-direction) and axial (x-direction) soil springs

2.1 Derivation of governing non-dimensional groups

Buried pipelines crossing active faults can be modeled as beams on elastic foundations. Steel pipelines in the field commonly have relatively small cross-sectional areas compared to distances along its axis (i.e. distance between supports). Therefore, they can be considered as slender beams and the Euler-Bernoulli beam approach can be used to model these pipelines. The soil surrounding pipelines is also assumed to be uniform. The governing differential equation of pipelines crossing active faults is very similar to the laterally loaded beam on elastic supports. The governing non-dimensional groups for the buried continuous pipelines crossing active faults can be derived by using either the governing differential or dimensional analysis. The details of the derivation of non-dimensional groups from the governing differential equations and the dimensional analysis can be found in the works of [15] and [23].

Non-dimensional groups derived from governing differential equations and obtained from dimensional analysis are given in Table 1. The values of these non-dimensional groups for selected field pipelines are given in Table 2.

Table 1 – Summary of non-dimensional groups identified using governing differential equations and dimensional analysis for studying soil-pipe interaction under faulting

Name of the non-dimensional group	**Physical Meaning**	**Remarks**
$\left(\frac{kD^4}{EI}\right)$	The flexibility of the pipeline so as to have similar soil-structure interaction	Small (kD^4/EI) : rigid pipe behaviour Large (kD^4/EI) : flexible pipe behaviour
$\left(\frac{T_u \times D^3}{EI}\right)$ or $\left(\frac{T_u \times D}{EA}\right)$	Normalized soil pipe friction	Axial pipe strains due to soil-pipe friction
$\left(\frac{D}{t}\right)$	The slenderness of the pipeline (affects pipeline failure mode)	Large (D/t): shell buckling failure mode Small (D/t): beam buckling failure mode
$\left(\frac{H}{D}\right)$	Non-dimensional burial depth (affects soil failure type)	Small (H/D): wedge type of soil failure Large (H/D): soil flow around the pipe
$\left(\frac{p}{\sigma_y}\right)$	Non-dimensional pipe pressure	The change in Hoop stress (This will influence the pipeline behavior under faulting)
$\left(\frac{\delta}{D}\right)$	Non-dimensional fault displacement (strain field in the soil around the pipeline)	Similar strain field will control soil-pipe interaction
β	Fault Crossing Angle	β:compression + bending - β: tension + bending

Table 2 – Values of non-dimensional groups for field pipelines

Non-dimensional group	Field (prototype) values (Range)	References
$\left(\frac{kD^4}{EI}\right)$	0.03-0.13	[24], [25], [26] and [18] (1971 San Fernando Earthquake, 1999 Chi Chi Earthquake, 1999 Kocaeli Earthquake)
$\left(\frac{D}{t}\right)$	72.4-125	
$\left(\frac{H}{D}\right)$	1.4-4	
$\left(\frac{\delta}{D}\right)$	1.4-5	
β	-90°< β<+90°	
$\left(\frac{p}{\sigma_y}\right)$	0.008-0.11 (maximum operating pressure is considered)	ASME (2006) and ASME (2007)

2.2 Scaling and design of experiment setup

2.2.1 Scaling of soil

The backfill material used in the experiments needs to be selected to ensure that the behavior of buried pipeline crossing faults is not influenced by grain size effects. The smallest ratio of the pipe diameter to average soil grain size (D/D_{50}) is chosen considering the criterion of $D/D_{50} \geq 48$ recommended by the International Technical Committee TC2 [27] based on centrifuge test data from [28] and [29]. Red Hill 110 Silica sand was used in the experiments. The relative density of the sand (D_r) is about 35%. Table 3 shows the engineering properties of Red Hill 110 dry sand. Figure 2 shows the particle size distribution of Red Hill 110 dry sand.

Table 3 – Values of non-dimensional groups for field pipelines

Properties	**Values**
Specific gravity	2.65
Median particle diameter D_{50} (mm)	0.144
Dry unity weight (kN/m^3)	13.0
Relative Density, D_r (%)	35
Peak internal friction angle (φ_{peak}) (°)	40
Residual internal friction angle (φ_{cv}) (°)	34
Dilation Angle (ψ) (°)	6
Maximum void ratio, e_{max}	1.035
Minimum void ratio, e_{min}	0.608

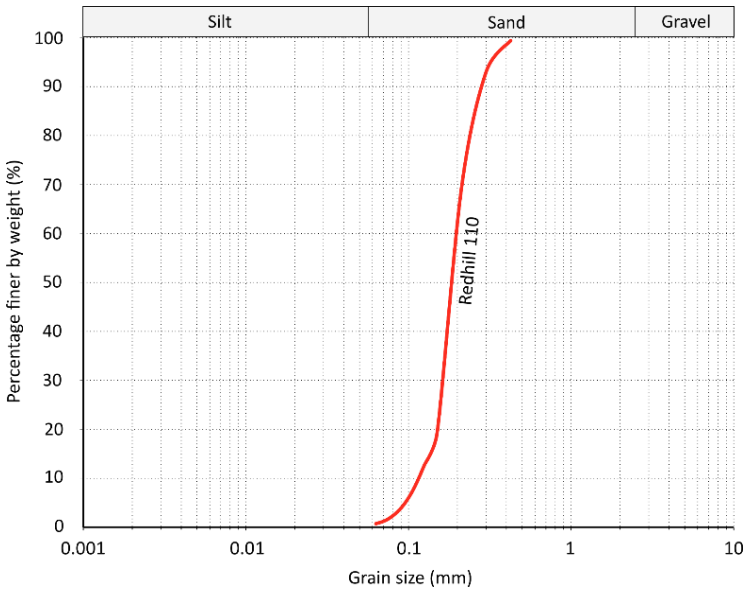

Fig. 2 – Particle size distribution of Red Hill 110 dry sand

2.2.2 Scaling of pipe diameter (D), pipe wall thickness (t) and burial depth (H)

Values of pipe diameter (D), pipe wall thickness (t) and pipe burial depth (H) used in the model tests were chosen considering relative soil-pipe stiffness (kD^4/EI) and the total curved length ($2xL_c$) of model pipelines crossing strike-slip faults. As seen in Table 2, the value of kD^4/EI in the field ranges between 0.03 and 0.13 so that this range will be considered in the model tests. Values of kD^4/EI in the model tests stay within this range. Furthermore, the total curved length ($2xL_c$) of model pipelines needs to be less than the total length of the test set-up in order to avoid boundary effects on the behavior of the model pipelines. The detailed information on the calculation of kD^4/EI and L_c can be found in the work of [23].

The ratio of pipe diameter to pipe wall thickness (D/t) and the ratio of pipe burial depth to pipe diameter (H/D) govern the type of pipeline failures so that these ratios need to be chosen considering the values observed in the field.

$$(D/t)_{model} \cong (D/t)_{field} \tag{1}$$

$$(H/D)_{model} \cong (H/D)_{field} \tag{2}$$

2.2.3 Scaling of fault movements

Fault displacements are assessed by the ratio of fault displacement to pipe diameters (δ/D) in order that the fault movement in the experimental model is of a comparable magnitude to field fault movements. Normalized fault displacements (δ/D) in the field for the selected cases range between 1.4 and 5.0 as seen in Table 2. The values of δ/D in model tests are selected considering this range and the fault movement (δ) in model tests is limited to 300 mm, resulting in a maximum δ/D of 6.

$$0 \leq (\delta/D) \leq 6 \tag{3}$$

2.2.4 Scaling of fault offset rate

As seen in the literature [20], the fault offset rate influences High-Density Polyethylene (HDPE) pipeline response to faulting. This is due to the strain rate dependent behavior of HDPE material. In model tests, the offset rate of 0.173 m/min was used. The upper bound for the expected prototype offset rate is about 60 m/min ([19]). Therefore, the offset rate used in the model tests is considered as slow compared to the prototype offset rate.

2.3 Experiment Setup

2.3.1 Physical Model

A physical model test setup was developed to investigate the buried pipeline response to strike-slip faulting. The test setup consists of two identical boxes: a) Fixed box and b) movable box. Figure 2a-c demonstrates side, front and plan views of the experiment setup with all components of the test setup. The dimensions of the split boxes are shown in Figure 2a-c. The total external dimensions of the model are 2000 mm length, 1000 mm width and 750 mm depth as seen Figure 2a-c. The internal dimensions of the model are 1950 mm length, 950 mm width and 700 mm depth.

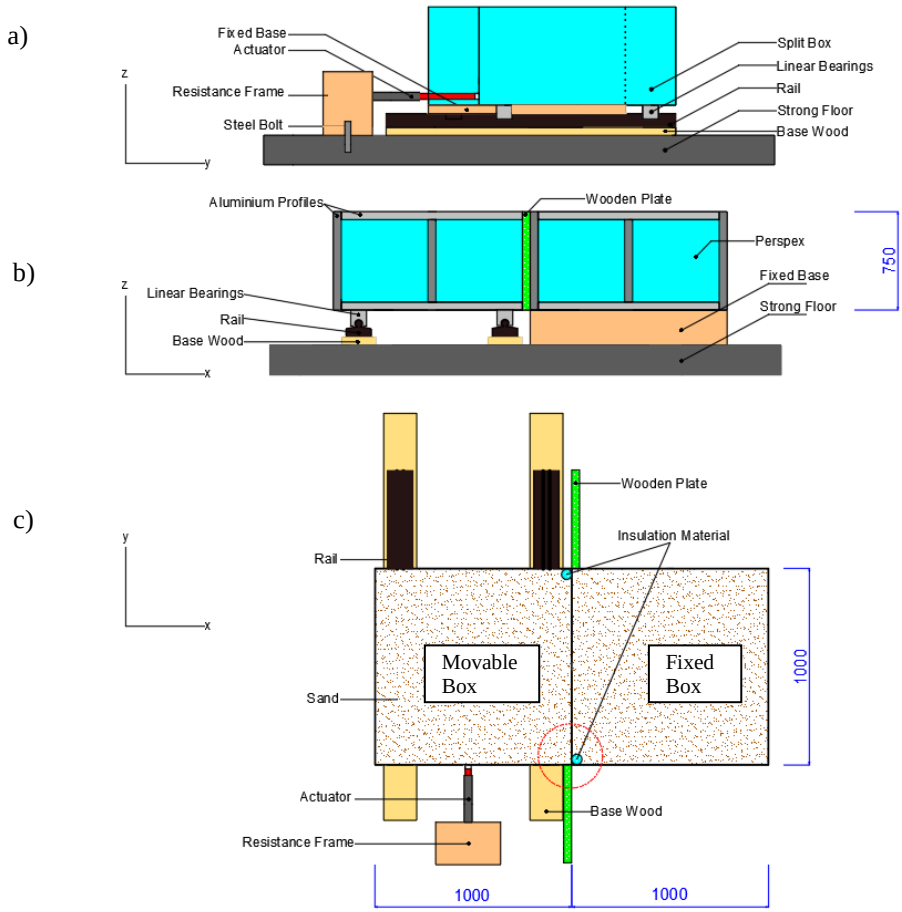

Fig. 3 – a) Side view of the experiment setup, b) front view of the experiment setup, c) plan view of the experiment setup

Linear bearings and rails were used to support and guide the movable box. This provides minimum friction and accurate movement. The base wood was used to flatten the surface underneath the split boxes. The rails were bolted on the wood bases. The wood bases were bolted to the strong floor. An electrical actuator system was used to displace the movable box up to a maximum of 300 mm. The linear actuator was linked to the movable box and resistance frame. The fixed box was constrained in every direction by bolting it to a fixed base. The fixed base was bolted to the strong floor as shown in Figure 2b.

The aluminum alloy struts with 40 x 40 mm cross-section and 8 mm groove were used to construct the frame of the split boxes. The side-walls of the split boxes were covered with perspex material with 6 mm wall thickness while the plywood material was used to cover the bottom of the split boxes. The plywood material was also used to prevent the sand from leaking out from the boxes (see Figure 2c). Pipe insulation foams

were also placed between sliding surfaces to prevent the sand from leaking as shown in Figure 2c. The outer diameter of the pipe insulation foam is 40 mm. The pipe insulation foams were compressed to provide tightness at the sliding surfaces.

2.3.2 Boundary effects

A 2m total length of the model was considered to be sufficient to avoid/minimize the effects of pipe end conditions on the bending response of the model pipelines. A newly developed end connectors were used at pipe ends to simulate equivalent boundary end springs. The end connectors were placed out of the curved zones (red section) as seen in Figure 4a. A schematic illustration of pipe end boundaries in the model tests is demonstrated in Figure 4b. More details about the design and construction of the proposed end connectors can be found in the work of [23]. Figure 4d shows the cross-section of the split box and minimum required distance of the centerline of the pipelines to the side boundaries ($L_{s,min}$) to avoid side-wall boundary effects on the pipeline response to faulting. Considering the work of [8], $L_{s,min}$ was selected as 250 mm ($L_{s,min}$ = 5D) and the minimum required distance of centerline of the pipelines to the bottom boundary ($L_{b,min}$) was selected as 125 mm ($L_{b,min}$ = 2.5D).

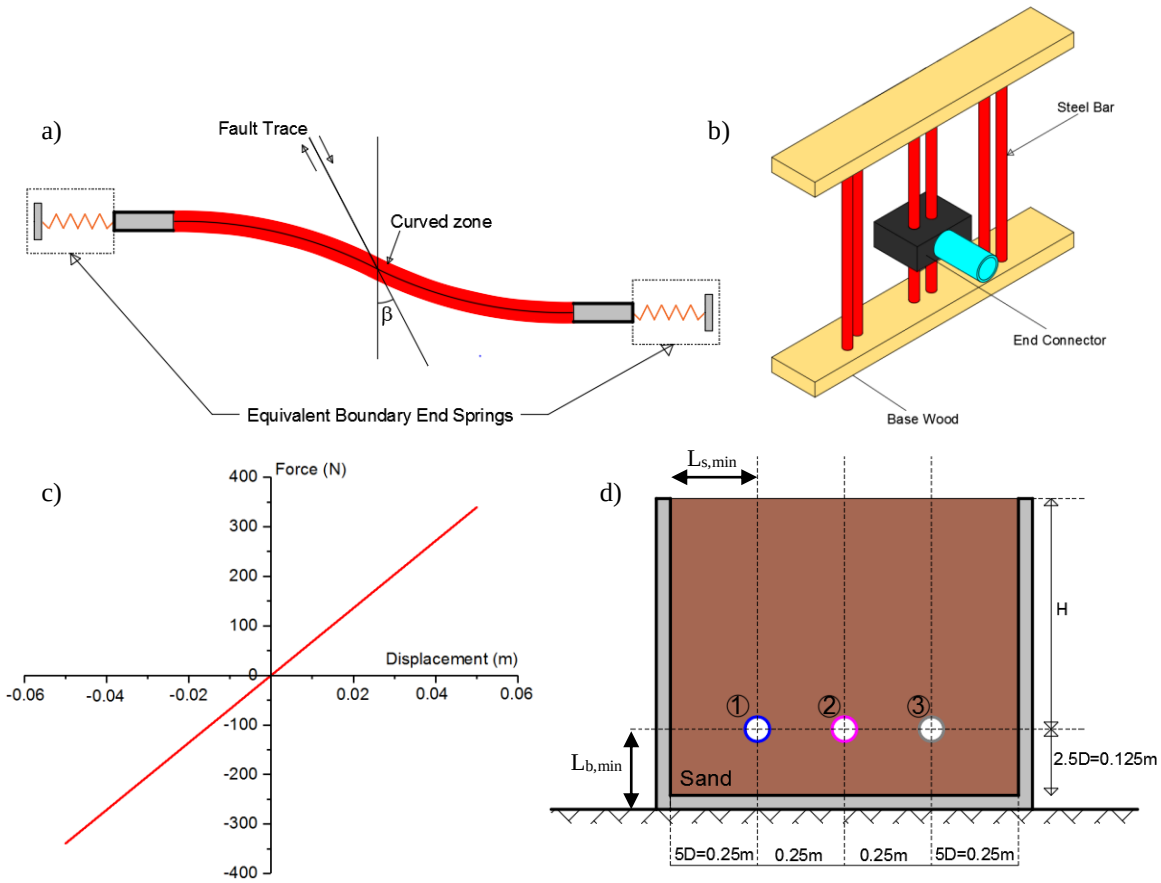

Fig. 4 – a) A schematic illustration of equivalent boundary end springs that are used to simulate pipe end conditions in the straight zone, b) a schematic sketch of pipe end boundaries in the model tests, c) force-displacement relationship for the proposed end connectors, d) the cross-section view of the experiment setup showing the minimum distance of the center of pipelines to the side boundaries

2.3.3 Instrumentation

The pipeline response to strike-slip faulting in terms of longitudinal strains was monitored by using five pairs of strain gauges along the pipe spring-lines as shown in Figure 5a-c. The axial strains (ε_a) are obtained by

calculating the average of longitudinal strains at spring-lines of the pipe while pipe bending strains (ε_b) are calculated as one-half the difference of longitudinal strains at spring-lines of the pipe.

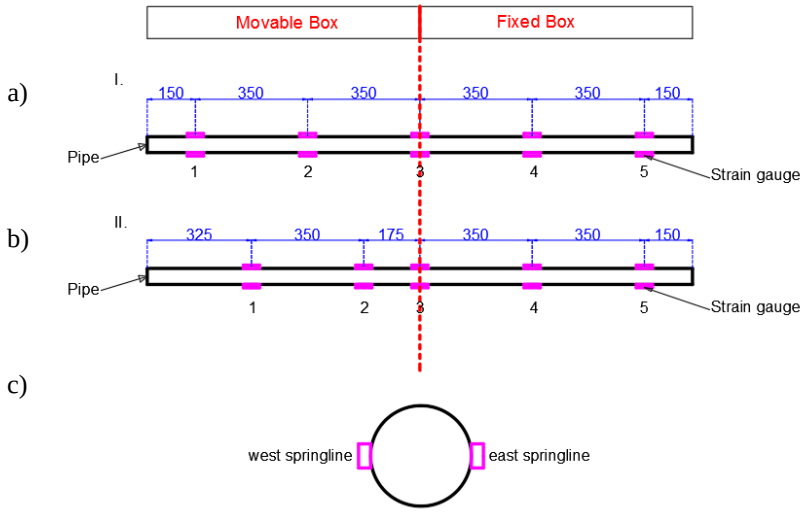

Fig. 5 – a) Strain gauge layout I, b) strain gauge layout II, and c) pipe spring-lines (dimensions in mm)

An S type beam load cell was attached between the tip of the actuator and the movable box to measure the load applied to the split box by the actuator. A Laser Displacement (LD) sensor was used to record the displacement applied to the movable box with time. Cameras were used for documentation purposes. Markers were placed on the ground surface to observe soil surface deformations in the plan. Figure 6 demonstrates a photo of the experiment setup showing frames, cameras, markers on the soil surface, the load cell and laser displacement sensor.

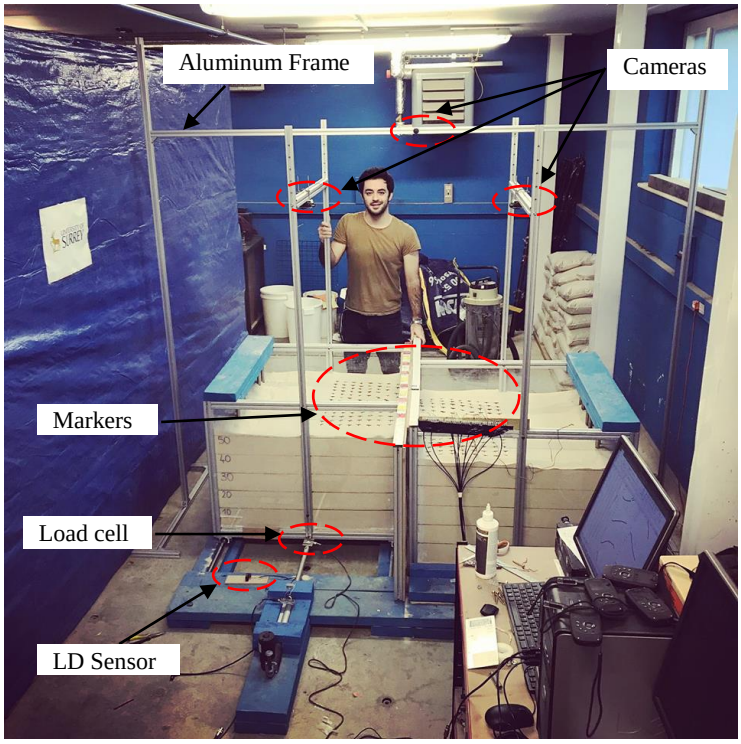

Fig. 6 – A photo of experiment setup showing frames, cameras, markers on the soil surface, load cell and laser displacement sensor

2.3.4 Experiment Plan

Four model tests with various pipe burial depths (H) and fault crossing angles (β) were performed to investigate the effects of H and β on the pipeline response to strike-slip faulting. These experiments were also performed to explore the reliability of the newly developed experiment. Table 4 shows the experimental plan summarizing various parameters used in model tests such as pipe materials, pipe diameters, pipe wall thicknesses, normalized burial depths, fault crossing angles and pipe end conditions.

Table 4 – Experimental plan summarizing pipe materials, pipe diameters, pipe wall thicknesses, normalized burial depths, fault crossing angles and end conditions used in the model tests

Test	Pipe Material	Pipe Diameter, D (mm)	Pipe wall thickness, t (mm)	H/D	Fault Crossing Angle (β), °	End Conditions
1	HDPE	50	3	5	90	End Connector
2	HDPE	50	3	7	90	End Connector
3	HDPE	50	3	7	15	End Connector
4	HDPE	50	3	7	-15	End Connector

3. Experiment Results

The axial strain distribution along the model pipeline for Test 1 is shown in Figure 7. The normalized pipe burial depth (H/D) in this test is equal to 5.0. Data points were obtained by strain gauges and trend-lines are plotted as seen in Figure 7. The trend-lines demonstrate that axial strains decrease with the distance along the pipeline.

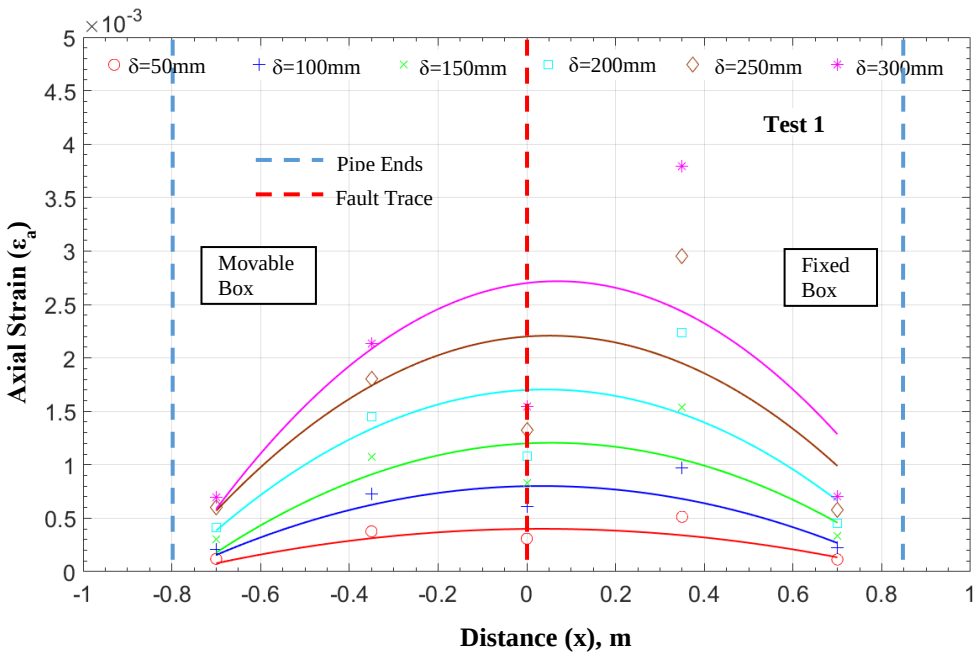

Fig. 7 – A photo of experiment setup showing frames, cameras, markers on the soil Surface, load cell and laser displacement sensor

Figure 8 shows the bending strain distribution along the pipeline for Test 1. The fault displacements used in this test range between 50 mm (δ/D=1.0) and 300 mm (δ/D=6.0). As seen in the figure, bending strains are approximately equal to zero at fault trace and bending strain distribution is symmetrical at around the fault trace.

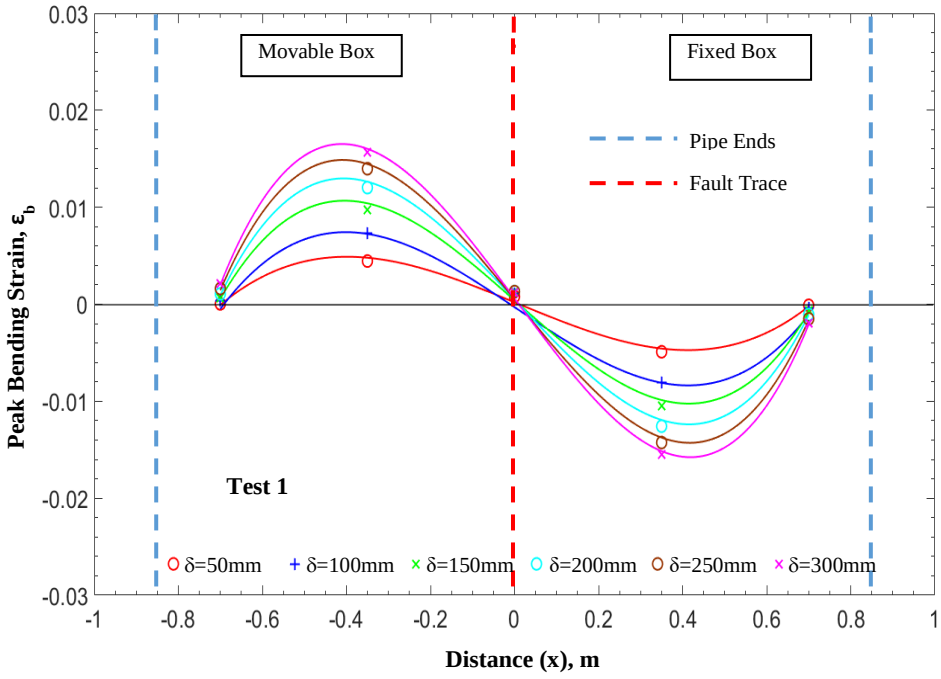

Fig. 8 – A photo of experiment setup showing frames, cameras, markers on the soil Surface, load cell and laser displacement sensor

The variation of peak bending strains with normalized fault displacements is plotted in Figure 9a while Figure 9b shows the variation of peak axial strains with normalized fault displacements. Peak bending strains sow logarithmic growth with the increase in fault displacements. Peak bending strains experience plateau with the increase in fault displacements since ultimate lateral soil resistance is reached.

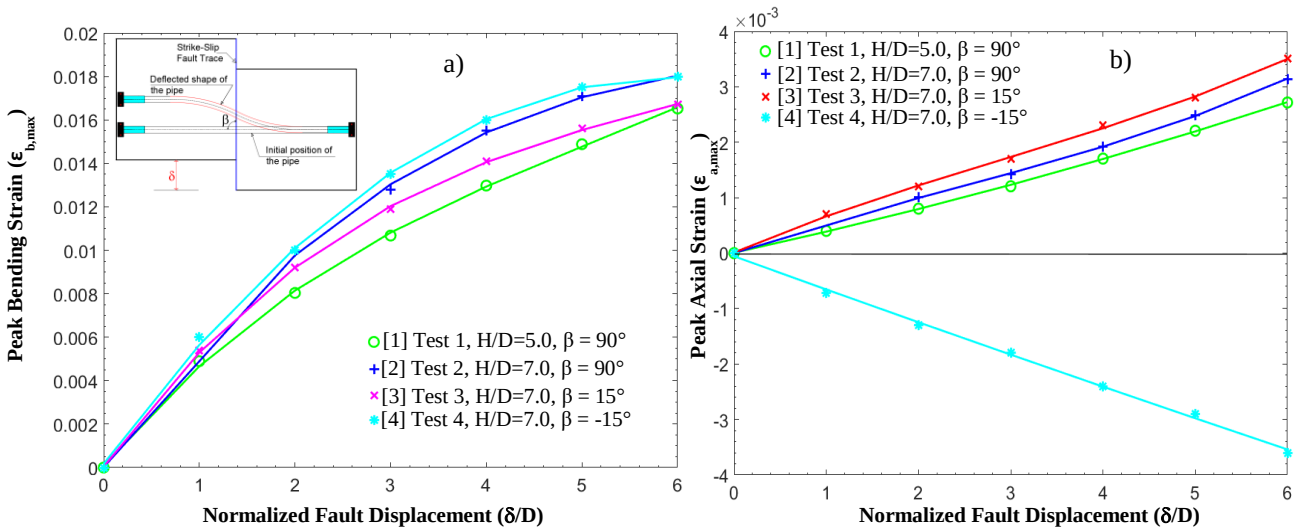

Fig. 9 – a) Peak Bending Strain vs. Normalized Fault Displacements, b) Peak Axial Strain vs. Normalized Fault Displacements

The increase in pipe burial depth (H) increases peak bending strains within the pipelines. Peak axial strains increase with the increase in the pipe burial depth. Relatively larger axial strains occur at +15° and -15° fault crossings compared to 90° of fault crossings. These findings are consistent with the results of earlier experimental studies.

4. Conclusions

The behavior of buried continuous pipelines crossing strike-slip faults observed in the model tests is similar to the behavior of full-scale pipelines observed in real earthquakes. Symmetric/Asymmetric (depending on the soil homogeneity at each side of the fault) double curvature bending with convex and concave shape occurs along the pipelines crossing strike-slip faults. Bending strains are equal to zero at the fault trace. The maximum axial strain occurs at the vicinity of the fault trace and it decreases along the pipeline. These observations are consistent with the earlier experimental studies and case studies. The increase in pipe burial depths results in the increase in both pipe bending and axial strains. Relatively smaller axial strains develop within pipelines when they cross fault with the fault crossing angle of 90°. Consequently, it can be suggested that pipelines should be buried at shallow depths at fault crossings and they should cross strike-slip faults with a fault crossing angle of 90° in order to increase pipeline performance under strike-slip faulting.

5. References

[1] Newmark NM, Hall WJ (1975): Pipeline design to resist large fault displacements. Proceedings of the U.S. National.

[2] Kennedy RP, Chow AW, Williamson RA (1977): Fault movement effects on buried oil pipeline. Transportation Engineering Journal, ASCE 103 (5), 617-633.

[3] Wang L, Yeh Y (1985): A refined seismic analysis and design of buried pipeline for fault movement. Earthquake Engineering and Structural Dynamics 13 (1), 75-96.

[4] Karamitros DK, Bouckovalas GD, Kouretzis GP (2007): Stress Analysis of Buried Steel Pipelines at Strike-slip Fault Crossings. Soil Dynamics and Earthquake Engineering, 27, 200–211.

[5] Karamitros DK, Bouckovalas GD, Kouretzis GP, Gkesouli V (2011): An Analytical Method for Strength Verification of Buried Steel Pipelines at Normal Fault Crossings. Soil Dynamics and Earthquake Engineering, 31(11), 1452-1464.

[6] Trifonov OV and Cherniy VP (2010): A semi-analytical approach to a nonlinear stress-strain analysis of buried steel pipelines crossing active faults. Soil Dynamics and Earthquake Engineering, 30(10), 1298-1308.

[7] Trifonov O, Cherniy VP (2012): Elastoplastic stress-strain analysis of buried steel pipelines subjected to fault displacements with account for service loads. Soil Dynamics and Earthquake Eng. 2012, 33(1), 54-62.

[8] Vazouras P, Karamanos SA, Dakoulas P (2010): Finite element analysis of buried steel pipelines under strike-slip fault displacement, Soil Dyn. Earthq. Eng., 30 (11), 1361–1376.

[9] Vazouras P, Karamanos SA, Dakoulas P (2012): Mechanical modelling of buried steel pipes crossing active strike-slip faults, Soil Dyn. Earthq. Eng., 41, 164–180.

[10] Vazouras P, Dakoulas P, Karamanos SA (2015): Pipe–soil interaction and pipeline performance under strike–slip fault movements, Soil Dyn. Earthq. Eng., 72, 48–65.

[11] Zhang L, Zhao X, Yan X, Yang X (2016): A new finite element model of buried steel pipelines crossing strike-slip faults considering equivalent boundary springs. Engng Struct., 123, 30 – 44.

[12] Gantes CJ, Melissianos VE (2016): Evaluation of Seismic Protection Methods for Buried Fuel Pipelines Subjected to Fault Rupture. Front. Built Environ. 2:34. doi: 10.3389/fbuil.2016.00034.

[13] Banushi G, Squeglia N, Thiele K (2018): Innovative analysis of a buried operating pipeline subjected to strike-slip fault movement. Soil Dynamics and Earthquake Engineering, 107, 234-249.

[14] Demirci HE, Bhattacharya S, Karamitros DK, Alexander N, and Singh RM (2018): Finite element model of buried pipelines crossing strike-slip faults by ABAQUS/Explicit. 16th European Conference on Earthquake Engineering, Thessaloniki, Greece.

[15] Demirci HE, Bhattacharya S, Karamitros DK, Alexander N (2018). Experimental numerical modelling of buried pipelines crossing reverse faults. Soil Dynamics and Earthquake Engineering, 114, 98-214.

[16] O'Rourke M, Vikram G, Abdoun T (2003): Centrifuge modeling of buried pipelines. Proceedings of the Sixth U.S. Conference and Workshop on Lifeline Earthquake Engineering, August 10-13, 2003, Long Beach, CA. 757-768.

[17] O'Rourke M, Gadicherla V, Abdoun T (2005): Centrifuge modelling of PGD response of buried pipe. Earthquake Eng. Eng. Vib., 4 (1), 69–73.

[18] Ha D, Abdoun TH, O'Rourke MJ, Symans MD, O'Rourke TD, Palmer MC, Stewart HE (2008): Buried high-density polyethylene pipelines subjected to normal and strike-slip faulting – a centrifuge investigation. Canadian Geotechnical Journal, 45, 1733-1742.

[19] Ha D, Abdoun TH, O'Rourke MJ, Symans MD, O'Rourke TD, Palmer MC, Stewart HE (2010): Earthquake Faulting Effects on Buried Pipelines-Case History and Centrifuge Study. Journal of Earthquake Engineering, 14:5, 646-669.

[20] Abdoun TH, Ha D, O'Rourke MJ, Symans MD, O'Rourke TD, Palmer MC, Stewart HE (2009): Factors influencing the modelling of buried pipelines subjected to earthquake faulting. Soil Dynamics and Earthquake Engineering, 29, 415– 427.

[21] Xie X, Symans MD, O'Rourke MJ, Abdoun TH, O'Rourke TD, Palmer MC, Stewart HE (2011): Numerical modelling of buried HDPE pipelines subjected to strike-slip faulting. Journal of Earthquake Engineering, 15(8), 1273– 1296.

[22] Sim WW, Towhata I, Yamada S (2012): One-g shaking-table experiments on buried pipelines crossing a strike-slip fault. Geotechnique, 62, 1067-1079, ISSN: 0016-8505.

[23] Demirci HE (2019): Experimental and numerical modelling of buried continuous pipelines crossing active faults, Doctoral thesis, University of Surrey.

[24] Southern California Gas Company (1973): Earthquake Effects on Southern California Gas Company Facilities. San Fernando, California Earthquake of February 9, 1971, Vol 2, U.S. Department of Commerce, Washington, D C., pp. 59-66.

[25] Schiff AJ, Tang AK (1999): Chi-chi, Taiwan, Earthquake of September 21, 1999: Lifeline Performance. Technical Council on Lifeline Earthquake Engineering (TCLEE) Monograph 18, American Society of Civil Engineers.

[26] Eidinger JM, O'Rourke M, Bachhuber J (2002): Performance of a pipeline at a fault crossing. 7th U.S. National Conference of Earthquake Engineering. July21–25, Boston. Earthquake Engineering Research Institute (EERI).

[27] International Technical Committee TC2 (2005): Catalogue of scaling laws and similitude questions in centrifuge modelling.

[28] Ovesen NK (1981): Centrifuge Tests of the Uplift Capacity of Anchor. Proc. Of the Tenth International Conference on Soil Mechanics and Foundation Engineering, Stockholm, pp.712-722.

[29] Dickin EA and Leuoy CF (1983): Centrifuge Model Tests on Vertical Anchor Plates, ASCE J Geotechnical Engineering, 109(12), 1503–1525.

[30] Bhattacharya S, Orense PR and Lombardi D (2019): Seismic Design of Foundations: Concepts and applications. Book, ICE Publications.

